ENVIRONMENTAL RESEARCH
LETTERS

LETTER • OPEN ACCESS

Estimates of temporal-spatial variability of wildfire danger across the Pan-Arctic and extra-tropics

IOP Publishing Environ. Res. Lett. 16 (2021) 044060 https://doi.org/10.1088/1748-9326/abf0d0

ENVIRONMENTAL RESEARCH
LETTERS

OPEN ACCESS

RECEIVED
8 January 2021

REVISED
7 March 2021

ACCEPTED FOR PUBLICATION
22 March 2021

PUBLISHED
12 April 2021

LETTER

Estimates of temporal-spatial variability of wildfire danger across the Pan-Arctic and extra-tropics

Flavio Justino[1,*], David Bromwich[2], Aaron Wilson[2,3], Alex Silva[4], Alvaro Avila-Diaz[1,4,5], Alfonso Fernandez[6] and Jackson Rodrigues[1,7]

[1] Universidade Federal de Viçosa, Departamento de Engenharia Agrícola, Viçosa, MG, Brazil
[2] Byrd Polar and Climate Research Center, The Ohio State University, Columbus, OH, United States of America
[3] OSU Extension—College of Food, Agricultural, and Environmental Sciences, The Ohio State University, Columbus, OH, United States of America
[4] Universidade Federal do Oeste do Pará, Instituto de Engenharia e Geociências, Santarem, PA, Brazil
[5] Natural Resources Institute, Universidade Federal de Itajubá, Itajubá, MG, Brazil
[6] Department of Geography, Universidad de Concepción, Concepción, Chile
[7] Universidade Federal Fluminense, Instituto de Educação de Angra dos Reis (IEAR), Angra dos Reis, RJ, Brazil
[*] Author to whom any correspondence should be addressed.

E-mail: fjustino@ufv.br

Keywords: fire danger, MODIS, vegetation, vulnerability

Supplementary material for this article is available online

Abstract

Satellite-based hot-spot analysis for the Pan-Arctic, shows that Asia experiences a greater number of fires compared to North America and Europe. While hot spots are prevalent through the year in Asia, Europe (North America) exhibits marked annual (semi-annual) variability. The Potential Fire Danger index (PFIv2) demonstrates increased fire incidence vulnerability across the Arctic and extra-tropics. Though not significant in northwestern North America and eastern Asia, significant-positive trends across the mid-latitudes of Eurasia and Siberia are clear. PFIv2 accurately matches the regional distribution of observed fires, while the worldwide used Fire Weather Index does not. Fire danger has evolved as distributions of short-interval precipitation events and background vegetation characteristics change. In conjunction with increased population and expanded infrastructure, frequent extreme events may increase pressure for new settlements that lead to greater fire exposure across the Pan-Arctic. Thus, PFIv2 may be useful for decision planners and danger managers to anticipate and minimize the adverse effects of indiscriminate fire use.

1. Introduction

Studies that anticipate the exposure of a region's fire occurrence are crucial to minimizing the harmful effect of fires [1–3]. Despite the threat posed by wildfires, there is a lack of systematic investigations focusing on wildfire danger, particularly across remote regions, such as the Pan-Arctic [4–9]. Identifying current and future patterns of fire incidence and hazard using a relatively simplified Fire Danger Index (FDI) formulation points out vulnerable regions. It thus is a valuable approach for local communities and authorities to predict and anticipate the potential occurrence of fires. Wildfires forecasts are a crucial day-to-day activity to management services and planning [4–9].

It should be emphasized that fire modeling is a complex task because it includes several parameters, such as soil characteristics, carbon allocation, and the moisture content of soil litter, that in most cases are very difficult to estimate or measure directly [10–14]. Fire ignition and spread depend on a combination of factors, and apart from human actions, weather features are the dominant drivers. This raises the need for a conceptual approach to be applied across limited data availability regions, such as the Pan-Arctic region.

Although most global wildfires have been observed in the tropics [3, 5], the Arctic and the extra-tropics have experienced an increasing number of wildfires in recent decades [6, 9]. Increased frequency of record-high temperatures, lack of precipitation (Prec), and deforestation due to human activity have higher environmental flammability [14–18]. Indeed, the hot and dry conditions across the western

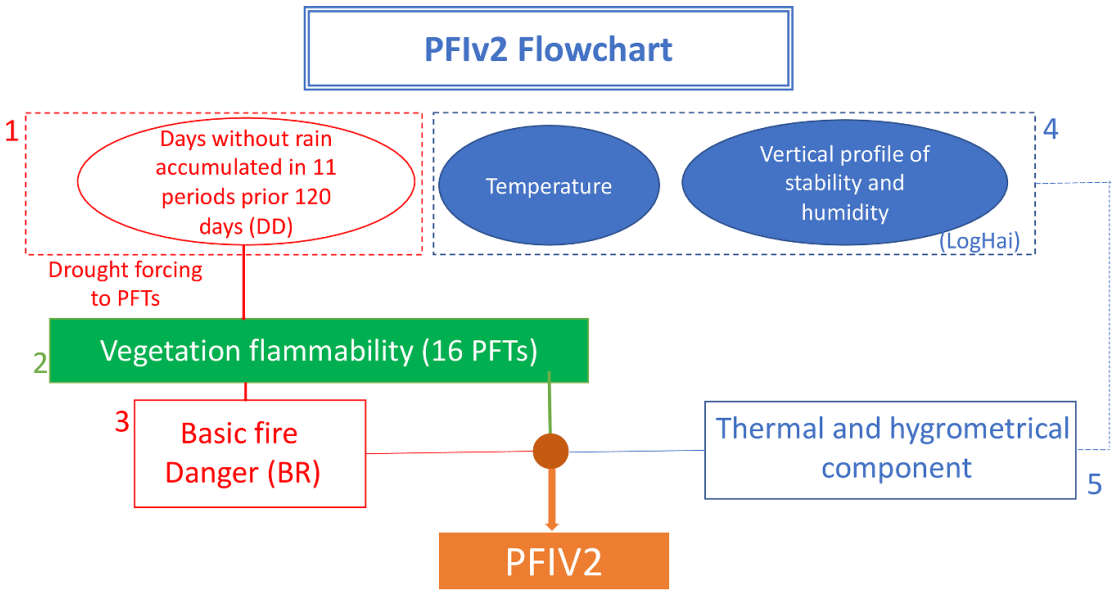

Figure 1. PFIv2 flowchart sequence for calculating the PFIv2 based on (3)(see section 2). Number indicate the sequence of steps to compute the PFIv2.

United States have allowed record-breaking megafires to occur in 2020, burning more than 33 000 km^2. In addition, southern Siberia has experienced many fires in high-density peatlands and permafrost [9, 10].

Weather observations and reanalyses (e.g. Arctic System Reanalysis version 2 (ASRv2) and ERA5) show that the magnitude of cold extremes (e.g. cold days, cold nights, frost days, ice days), have decreased substantially for the period 2000–2016 across the North American Arctic [15, 16]. Whereas the maximum and minimum temperatures display upward trends ranging between 0.5 °C and 0.7 °C decade^{-1}, the warming pattern is also associated with an increase in consecutive dry days and a reduction in total wet days over the Arctic basin. Importantly, fire incidence appears to increase over regions with dry and hot climate trends, usually through the occurrence of short (e.g. extreme maximum temperature, heatwaves) and medium-term (e.g. droughts) climate extremes [16–18].

The current study explores the capability of the Potential Fire Index version 2 (PFIv2, figure 1) to verify: (a) the variability of hot-spots across the Pan-Arctic in order to assess the dominant pattern of wildfire frequency in both time and space; (b) by applying two high resolution reanalyses (ASRv2 and ERA5) is verify the capability of the PFIv2 to reproduce regions with large number of hotspots; and (c) the PFIv2 is compared to the worldwide used Fire Weather Index (FWI), aiming at determining the reliability of these FDIs to match MODIS hotspots.

North America, Europe, and Asia are individually studied regarding the spatial hot-spots patterns, distribution of hot-spots as a function of vegetation, and the performance of each method in reproducing/matching areas with fires. Regions have been investigated considering their particular characteristics of both climate and vegetation. Due to the dynamic aspect of climate conditions, it is important to have a hemispheric picture of the fire danger. This helps to identify differences in the seasonal behavior of the fire activity and their link to climate patterns.

2. Materials and methods

The calculation of the wildfire danger has currently been carried out globally using reanalyses. Two high-resolution products are applied to compute the wildfire danger: ASRv2 and ERA5. These reanalyses have a close agreement with observed Prec, temperature, and other surface variables, including winds [16, 19, 20].

2.1. The Arctic System Reanalysis version 2 (ASRv2)

ASRv2 is a multi-agency, university-led retrospective analysis (reanalysis) of the Greater Arctic for 2000–2016. The ASRv2 has 15 km horizontal resolution, 29 pressure levels (71 model levels), 27 surface and 10 upper air analysis variables, 74 surface and 16 upper air forecast variables, and 3 soil variables. The higher horizontal resolution and weekly modification of the vegetation cover based on satellite data in ASRv2 better captures the small scale-processes associated with day-to-day vegetation feedbacks that are extremely important for wildfire behavior.

2.2. The European centre for medium-range weather forecasts (ERA5)

ERA5 provides hourly estimates of many atmospheric, land, and oceanic climate variables for 1950–present. The data cover the Earth on a 30 km grid and

resolve the atmosphere using 137 levels from the surface up to a height of 80 km. Surface data are also available, containing 2D parameters such as Prec, 2 m temperature, top of atmosphere radiation, and vertical integrals over the entire atmosphere.

2.3. Potential weather fire index version 2 (PFIv2)

The PFIv2 is primarily based on the assumption that fire danger increases according to the distribution of dry periods [3] as a function of the local vegetation type. The accumulated rainfall is distributed in 11 periods within the last 120 d, prior to the day of interest, this is namely: the days of drought (DD). This factor estimates the impact of dry spells on the PFIv2 [3, 21]. The computation of Prec in periods such as 1, 2, 3, 4, 5, 6–10, 11–15, 16–30, 31–60, 61–90, and 91–120 d is important, because for instance, 5 mm of rainfall within 1–5 d before the day of interest to estimate the fire danger, may not be sufficient enough to reduce the environmental flammability (box 1 in figure 1). Thus, it is crucial to determine the distribution of accumulated Prec in distinct intervals. The formulation to compute these precipitation factors (PF) is shown below, and the parameterization is used to characterize the influence of vegetation types in the fire danger (PFIv2).

$$\mathrm{DD} = 105 \times (\mathrm{PF}_1 \times \mathrm{PF}_2 \cdots \times \mathrm{F} = \mathrm{PF}_{91-120}), \quad (1)$$

where $\mathrm{PF}_1 = \mathrm{e}^{(-0.14\mathrm{Prec})}$, $\mathrm{PF}_2 = \mathrm{e}^{(-0.07\mathrm{Prec})}$, $\mathrm{PF}_3 = \mathrm{e}^{(-0.04\mathrm{Prec})}$, $\mathrm{PF}_4 = \mathrm{e}^{(-0.03\mathrm{Prec})}$, $\mathrm{PF}_5 = \mathrm{e}^{(-0.02\mathrm{Prec})}$, $\mathrm{PF}_{6-10} = \mathrm{e}^{(-0.01\mathrm{Prec})}$, $\mathrm{PF}_{11-15} = \mathrm{e}^{(-0.008\mathrm{Prec})}$, $\mathrm{PF}_{16-30} = \mathrm{e}^{(-0.004\mathrm{Prec})}$, $\mathrm{PF}_{31-60} = \mathrm{e}^{(-0.002\mathrm{Prec})}$, $\mathrm{PF}_{61-90} = \mathrm{e}^{(-0.001\mathrm{Prec})}$, and $\mathrm{PF}_{91-120} = \mathrm{e}^{(-0.0007\mathrm{Prec})}$.

Basic danger (BR) for individual vegetation types is calculated as:

$$\mathrm{BR}n = 1,16 = 0.9 \times (1 + \sin(An = 1,16 \times \mathrm{DD}))/2, \quad (2)$$

where $An = 1,16$ is the type of vegetation (boxes 2 and 3 in figure 1).

The PFIv2 also considers surface temperature, the type, and natural cycle of vegetation defoliation, the vapor pressure deficit (VPD), and the atmospheric stability at the lower atmosphere from the surface to 700 hPa (LogHai factor; figure 1 boxes 4, 5, and equation (3)).

$$\mathrm{LogHai} = \left\{ \begin{array}{c} 7 \times 10^{-5} \times W^3 - 0.0035 \times W^2 + 0.072 \times W - 0.26, \ \text{if elevation} \leqslant 1500\,\mathrm{m} \\ 1 \times 10^{-4} \times W^3 - 0.0056 \times W^2 + 0.115 \times W - 0.53, \ \text{if } 1500\,\mathrm{m} \leqslant \text{elevation} \leqslant 3500\,\mathrm{m} \\ 9 \times 10^{-5} \times W^3 - 0.0065 \times W^2 + 0.196 \times W - 1.89, \ \text{if elevation} \geqslant 3500\,\mathrm{m} \end{array} \right\} \quad (3)$$

The W considers the specific humidity and air stability as a function of vertical atmospheric layers based on the Haines Index [3]. This is important because it incorporates local elevation characteristics into the method. A systematic evaluation of the global performance of the PFIv2 on reproducing regions with the highest concentration of fires [3] demonstrates that PFIv2 delivers efficiency of up to 80% in matching the observed fires from the Terra/MODIS satellite. The PFIv2 concerning MODIS burned areas (BAs) reveals correlation values greater than 0.6 over the most susceptible regions, such as Africa and South America.

The effect of air temperature (FT) is included as:

$$\mathrm{FT} = (0.02 \times Tx + 0.4) \times (0.003\,|\mathrm{Lat}| + 1), \quad (4)$$

where $|\mathrm{Lat}|$ is the latitude module, and Tx is the daily maximum temperature.

Finally, the PFIv2 is computed as:

$$\mathrm{PFIv2} = \mathrm{BR} \times (a \times \mathrm{LogHai} + b) \times \mathrm{FT}, \quad (5)$$

where $a = 0.006$ and $b = 1.3$.

The PFIv2 attains values from 0 to 1, which is represented follows the assumption in equation (2), which considers the link between the vegetation and DD as a sine function, and equation (3) that is limited by a logistic function. The categories of PFIv2 are five on a scale of 0–1, such as: minimum, below 0.15; low, from 0.15 to 0.4; medium, from 0.4 to 0.7; high, from 0.7 to 0.95 and; critic, above 0.95. Those classes were defined based on the percentage of fires that are detected on these PFIv2 intervals.

The present PFIv2 calculation across the Pan-Arctic and extra-tropics differs from Silva *et al* [3], because it includes annual vegetation patterns based on MODIS observations during 2001–2016. It might be expected that the PFIv2 will reproduce changes in fire danger throughout the years related to the conversion of forests to savannas, pasture/grassland, or other biomes more prone to fire development. This variable is generated from annual MODIS MOD12C1 (https://lpdaac.usgs.gov/products/mcd12c1v006) and MCD12Q1 (https://lpdaac.usgs.gov/products/mcd12q1v006/) product observations, available from the Land Processes DAAC.

2.4. Forest fire weather index (FWI) system

The FWI [22] utilized here is based on the ERA5 dataset used at ECMWF/Copernicus Climate Change

Services (https://climate.copernicus.eu/fire-weather-index). The FWI is extensively applied by National Weather Service worldwide to estimate fire danger. The FWI applies three moisture indices: The Fine Fuel Moisture Code, representing the moisture content in fine fuels, the Duff Moisture Code to parameterize organic material, and the Drought Code, which is a deep layer of compact organic material.

2.5. Satellite detected hot-spots (MODIS)

The MODIS-based hot-spots product combined (Terra and Aqua) MODIS NRT active fire products (MCD14DL) processed using the standard MOD14/MYD14 Fire and thermal anomalies algorithm available at https://earthdata.nasa.gov/earth-observation-data/near-real-time/firms at 1 km resolution from 2001 to 2016, have been used as fire proxies.

It has to be mentioned that hot-spots may display false identification of actual fires. However, previous studies such as Giglio *et al* [23], Friedlingstein *et al* [21], Roteta *et al* [24], and Curworth *et al* [25] have demonstrated that the large majority of hot spots matches actual fires, in particular after the use of the MOD14/MYD14 re-calculation. Certainly, mismatches between real fires and hot spots can occur due to detection at industrial and oil chimney, volcanic areas, and large sand banks, for instance. However, analyses of the last two decades in Brazil have shown very reliable identification of fires based on MODIS products (https://queimadas.dgi.inpe.br/queimadas/bdqueimadas). Moreover, it has been found that those spurious fires/false alarms represent very little of the total detection. In this sense, we argue that a substantial drawback does not arise from using MODIS products.

2.6. Statistical analyses

Abrupt changes in the time series are detected using the Pettitt homogeneity test [26]. We used the Sen slope [27] method to estimate the increase or decrease per unit of the time series. The Sen slope is an unbiased estimator of linear regression slope, which is less sensitive to extreme values. Furthermore, the Mann–Kendall test was used to determine the time series statistical significance [28, 29]. These non-parametric tests do not require a hypothesis in the data distribution. They have been extensively used to detect and estimate trends in extreme values in atmospheric and hydrological variables and radiative fluxes [30, 31]. We set the significance level for the Mann–Kendall and Pettit analysis to 0.05 and 0.1.

3. Results

3.1. Satellite-based interannual fire variability

Most fires in the Northern Hemisphere are concentrated in the summer and spring months (figures 2(C), (F) and (I)). On the other hand, minimal fire activity usually occurs from November to February (NDJF) during the period of greatest snow cover, high relative humidity, and coldest temperatures [3]. Fires during NDJF account for only 10% of the total annual occurrence (figures 2(A), (D) and (G)).

In order to verify in more detail, the Arctic and extra-tropics have separated in North America, Europe, and Asia (figure S1(A) (available online at stacks.iop.org/ERL/16/044060/mmedia)). It is interesting to note that fires in Europe tend to peak during the summer months, with a secondary peak in March–April in some regions. The number of annual fires in Asia can reach values up to 400 000, whereas in North America and Europe, the numbers are fewer than 120 000. However, it is not straightforward to detect an increase or reduction in the number of fires because the time series are still too short of providing robust statistics (figure 2).

The annual cycles of the total number of fires in the Arctic and extra-tropics (2001–2016) show inherent characteristics to Asia, Europe, and North America, respectively (figures 2 and S1). In Asia, seasonal changes in fires are not well defined because hot spots are present throughout the year, except from December to February. This is not the case in North America, where there is a dominant peak in JJA, revealing the enhanced seasonality dominance. This feature results from the massive concentration of fires in the western part of North America.

In Europe, the semi-annual cycle is particularly noticeable with two maxima (minima) in March–April (May–June), and July–August (November–February). Hantson *et al* [4] also found a double peak in BAs in the northern extra-tropics. Indeed, our analysis confirms this seasonality and is primarily dictated by the fire activity in Europe. Similar behavior is delivered by the monthly standard deviation (STD) in the sense that the magnitude of monthly fluctuations in fire incidence follows the long-term seasonal pattern (figure S1).

Figure 3 shows the spatial distribution of hot spots north of 40° N. In the Pan-Arctic, fires frequently occur across Canada/Alaska and eastern Siberia; however, the most considerable incidence is found along the border between Russia and Mongolia/China (100–120° E). Central Asia also exhibits intense fire activity (figure 3(A)). Most fires are related to land preparation for agricultural activities, but the role of lightning should not be disregarded, particularly across eastern and southern Europe and eastern Asia. In central Asia, long summers and short winters induce rapid growth of grasslands that increase the amount of combustible material.

The STD (figure 3(B)), shows that the number of fires fluctuates substantially throughout the years and months. This is indicated by the spatial match between the highest STD and the number of hot spots. Departure from mean conditions is related to

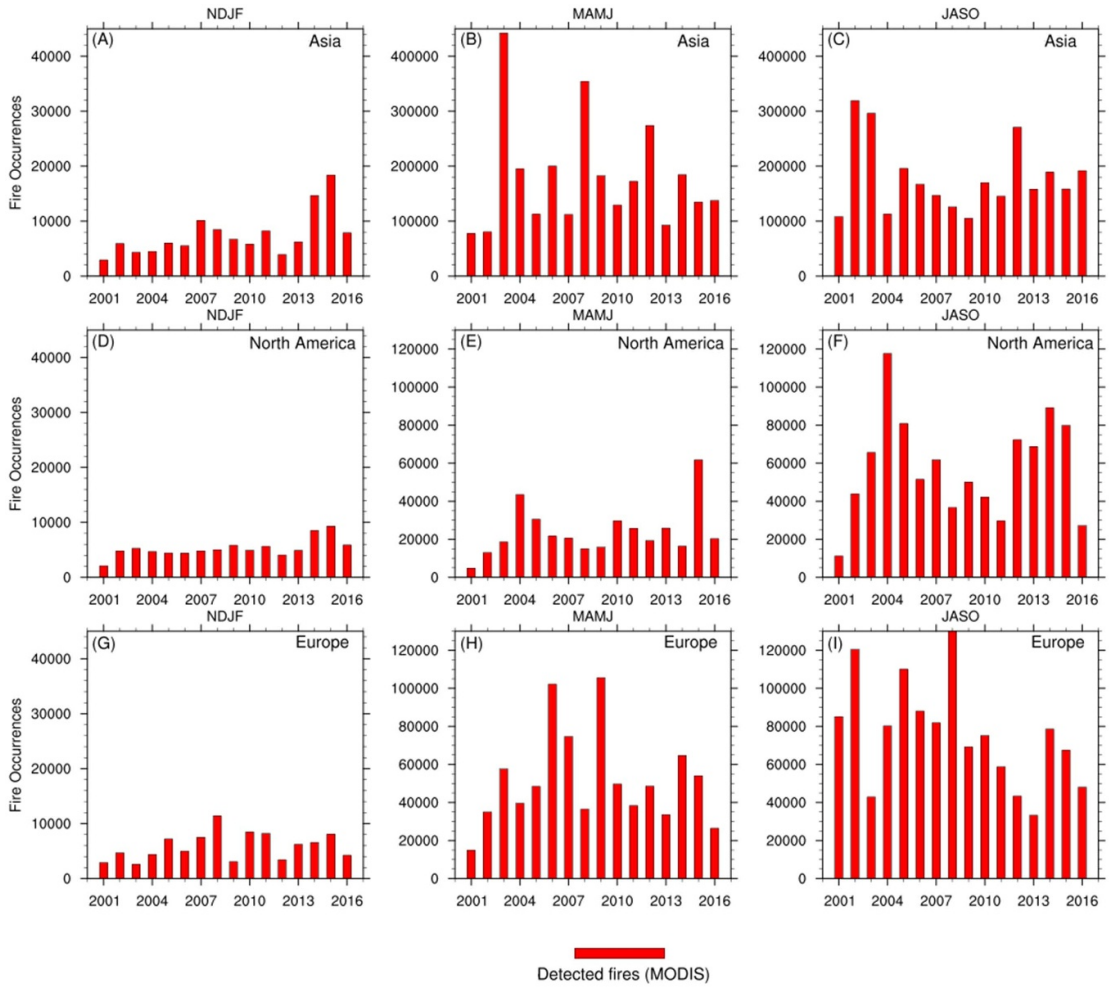

Figure 2. Interannual variability of fire as detected by MODIS. Column 1 is for NDJF, column 2 for MAMJ, and column 3 for JASO for (A)–(C) Asia, (D)–(F) North America, and (G)–(I) Europe. Note that the *y*-axis differs among the individual panels.

factors such as human actions, lightning, land use changes, and the persistence of extremes events such as heatwaves and dry spells [32]. These latter weather events lead to vegetation browning through increased plant thermal and water stresses that favor fire events [33, 34].

The temporal evolution of the hot spots demonstrates that increased fire activity has occurred mostly in the western part of North America, central Asia, and China (figure 3(C)). In Asia, it is clear that more than 60% of fires occur in four vegetation classes (woody savannas, savannas, croplands, and grasslands), but approximately 7% of fires are located in mixed forests (figures 3(D) and 4(A)). In North America, hot spots are mostly found in the same four vegetation classes as in Asia, though other vegetation types are also affected (e.g. evergreen needleleaf forests (figures 3(D) and 4(B))). These biomes store huge quantities of carbon and are home to diverse fauna and flora. Fire characteristics in Europe are different because the greatest number of fires (up to 60%) are concentrated in crop production regions (figure 4(E)). Evaluation of the temporal changes reveals that the incidence of fires in Asia on grasslands has decreased for 2001–2016. In North America, marked positive trends in four vegetation classes (table 1) highlight temporal links between hot spots and vegetation.

Trends of monthly accumulated hot spots (figures 3 and 4) and potential change points for most represented vegetation classes across the Pan-Arctic are shown in table 1. Mann–Kendall and Sen Slope tests have been used to calculate the statistical significance and magnitude of trends. The robustness of trend values derived from the monthly time series for 2001–2016 might be questionable. Nevertheless, there is no consensus on the minimum length of a time series applied in trend calculations [35–37]. Two previous studies have analyzed the time series with different intervals, using Landsat imagery (1995–2010) and MODIS EVI data from 2001 to 2014 [18, 38]. These analyses demonstrate the robustness of those change-points, trends, and seasonality analyses despite having only two decades of data.

Pettitt's test indicates statistically significant break/abrupt change in the fire time series pattern in North America (June 2002) and Asia (October 2010). According to NOAA, 2010 was the warmest year on

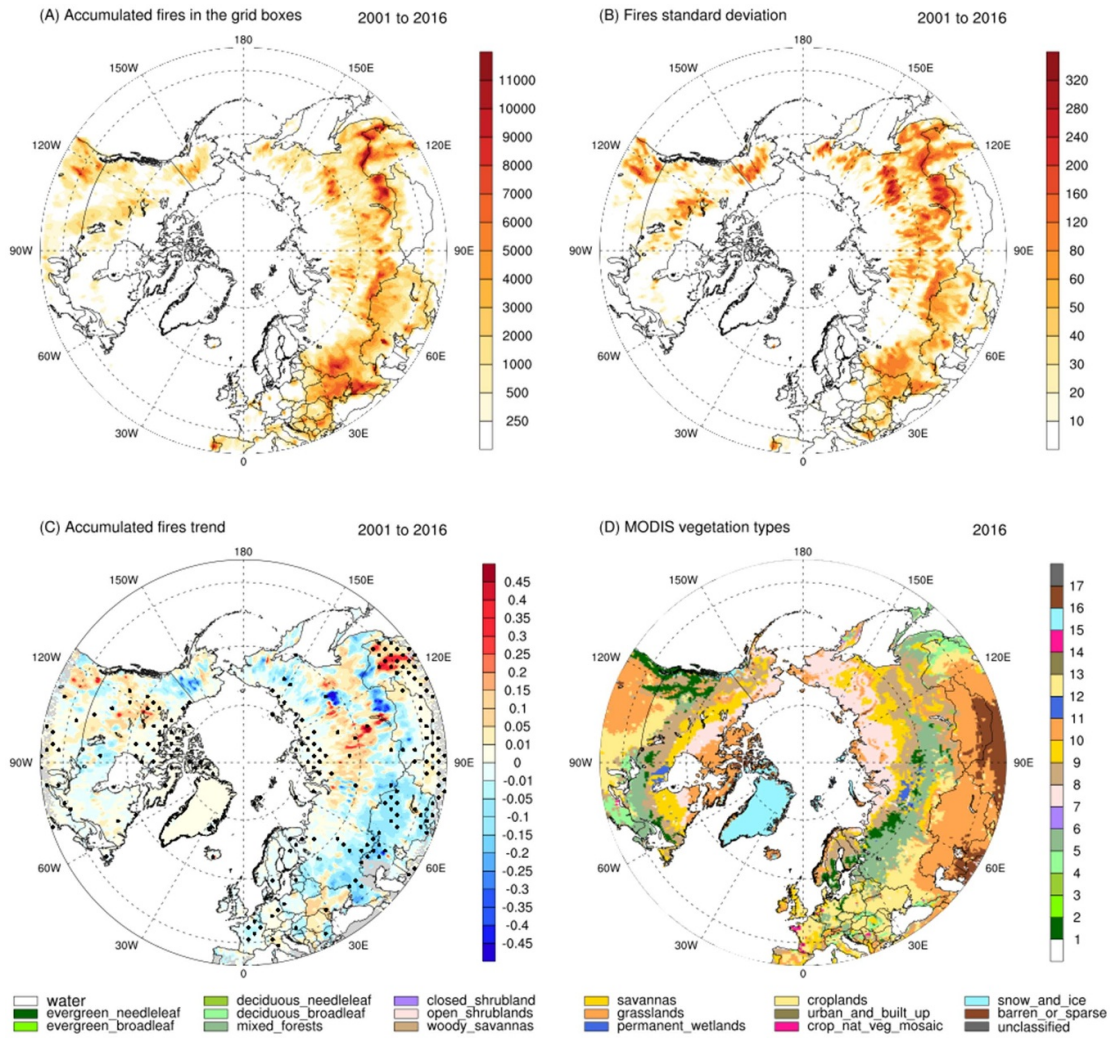

Figure 3. Observed fire characteristics across the Pan-Arctic for 2001–2016. (A) Accumulated fires in 1° × 1° (latitude, longitude) grid box. (B) Monthly standard deviation of fires. (C) Accumulated fire trends. (D) MODIS vegetation types. Dotted regions are significant at 90% level.

record since 1901 across India and parts of central Asia [33, 34]. This was also accompanied by more heat waves. This is the likely cause for change point detection. The magnitude and slope are significant at the 90% confidence level over North America in regions dominated by evergreen needleleaf, woody savannas, grasslands, and cropland.

In 2002, North America experienced drought conditions across one-third of the United States, most intense across the eastern seaboard and in the northwest [34]. This resulted in an early wildfire season and the largest area burned in the past 50 years. In Europe, trends are positive except over woody savannas and grasslands. In Asia, trends are mostly positive as well, except in the grasslands of central Asia, where the number of fires has decreased over the last two decades.

The overall trend patterns demonstrate an increase in fire activity in evergreen needleaf, woody savannas, cropland, and grassland domains. However, changes in local population growth over the last two decades, even in increased migration, do not match regions with trends in satellite detected-hot spots. Thus, a systematic understanding of the role of climate evolution in changes of fire incidence (trends) is extremely valuable. A proper estimate of environmental and vegetation fire dangers allows for adequate mitigation of vegetation fires' destructive effects, thereby reducing economic and human losses.

3.2. Spatial distribution of PFIv2 (ASRv2 and ERA5 datasets)

PFIv2 and its components based on ASRv2 regional reanalysis show that during the summer season, large areas of the Northern Hemisphere are susceptible to fire activity (figure 5). The basic danger (figure 5(A)) shows very critical conditions across the Canadian Arctic and northern Asia in the Russian Federation. These regions are dominated by savannas, open shrublands, and grasslands (see figure 1(A) in [3]) and experience intervals without Prec. Increased fire danger also appears in the mid-latitudes of western North America, over most of Europe, and central

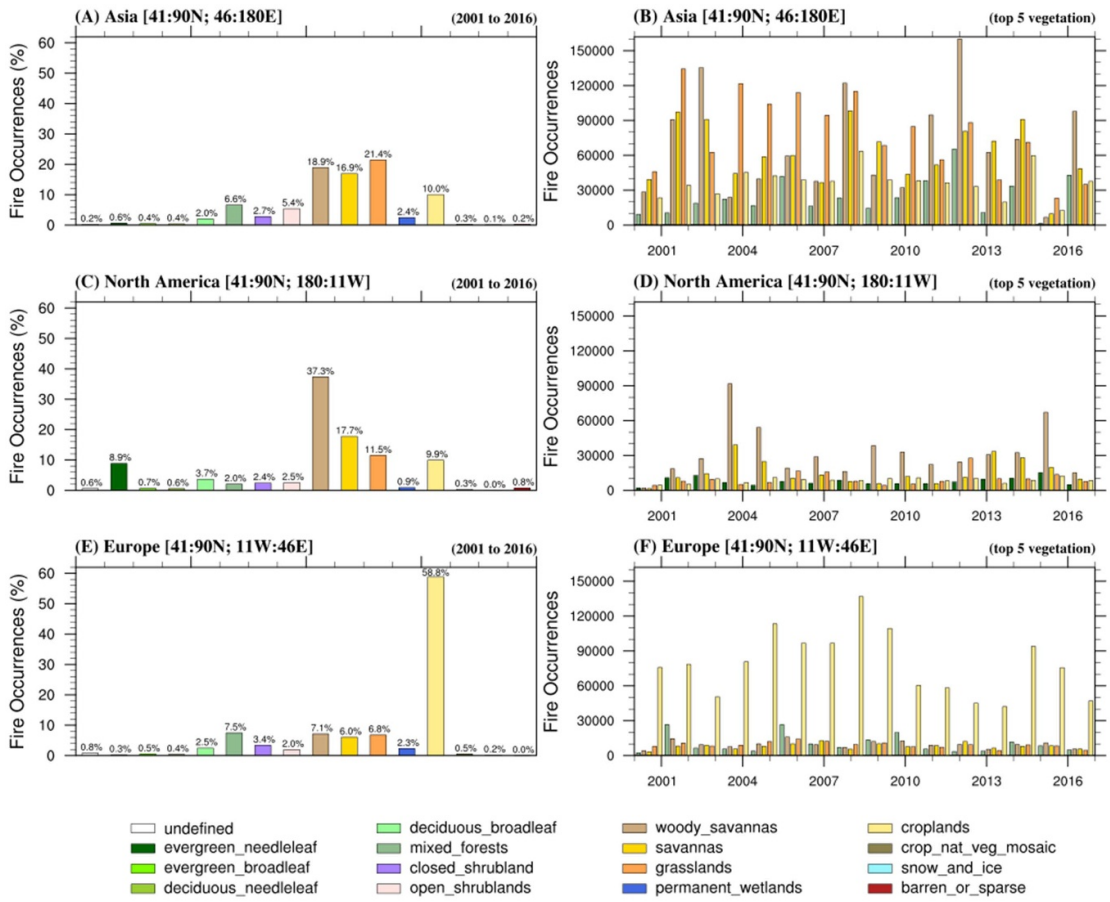

Figure 4. Relationship between satellite-detected fires and vegetation types. (A), (C), and (E) show the total number of fires in 2001–2016 for each biome for Asia, North America, and Europe, respectively. (B), (D), and (F) display the annual evolution of fires within the five most representative biomes for Asia, North America, and Europe, respectively.

Table 1. Trends and abrupt change points for satellite-based fires. Results show fires during 2001–2016 in the five most representatives vegetation classes. Values marked in bold are statistically significant at the 90% level.

	Vegetation	Abrupt change (pettitt test)		Trend	
		P-value	Month—Year	*P*-value	Trend (month)
North America	Evergreen needleleaf	**0.0940**	**Jun-2002**	**0.0474**	**0.5579**
	Woody savannas	0.1320	May-2004	**0.0847**	**0.7667**
	Savannas	0.4930	Mar-2003	0.3534	0.0781
	Grasslands	0.2590	Jun-2002	**0.0651**	**0.7203**
	Cropland	0.4020	Feb-2005	**0.1072**	**0.6315**
Europe	Mixed forests	0.9700	Feb-2014	0.9070	0.0118
	Woody savannas	0.8630	Feb-2002	0.9633	−0.0136
	Savannas	0.4100	Feb-2005	0.2685	0.4444
	Grasslands	0.4680	Oct-2012	0.4363	−0.3622
	Croplands	0.6130	Jun-2004	0.7685	0.6704
Asia	Mixed forest	0.6110	Mar-2010	0.4109	0.4615
	Woody savannas	0.4300	Mar-2011	0.3249	0.2359
	Savannas	0.8810	Agu-2009	0.5990	−0.0467
	Grasslands	**0.0850**	**Oct-2010**	**0.0791**	**−8.047**
	Croplands	0.7830	Feb-2014	0.2774	1.3563

Asia (figure 5(A)). In the mid-latitudes, the PFIv2 term that includes the VPD and atmospheric stability (LogHai, (figure 5(B))), is in line with greater fire danger. Drier atmospheres may result in increased evapotranspiration that affects vegetation greening/wetness [38].

The surface temperature may also increase the PFIv2 (figure 5(C)), but in locations where conditions related to Prec and atmospheric humidity are not favorable for fire activity, the former effect alone cannot result in greater fire danger. The combined effect of forcing that contributes to the PFIv2 is shown

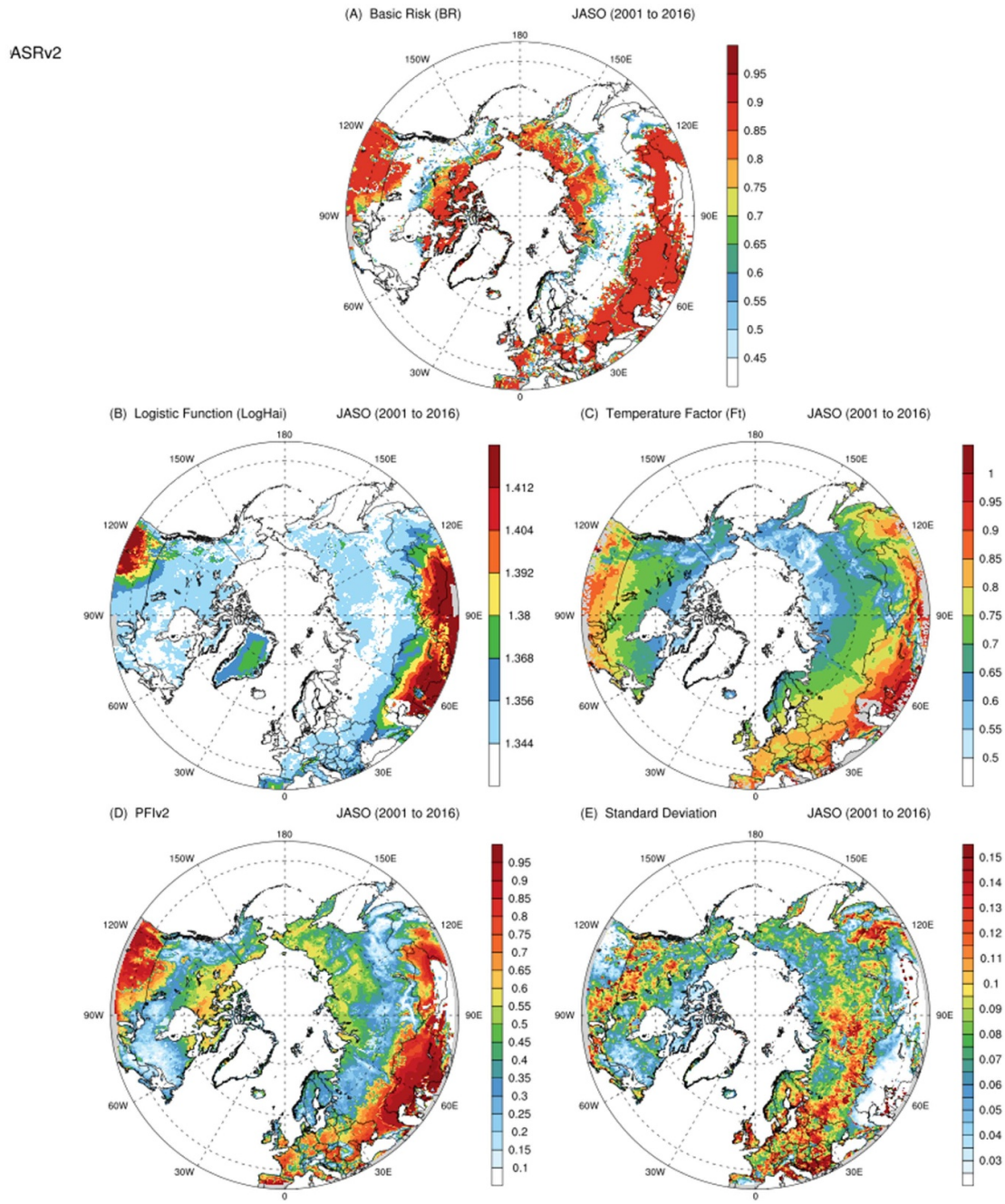

Figure 5. PFIv2 components. (A) Basic danger. (B) LogHai. (C) Surface temperature term. (D) PFIv2. (E) shows the PFIv2 standard deviation based on ASRv2 for the 2001–2016 interval.

in figure 5(D). It is clear that the number of dry days (figure 5(A)) exerts the dominant role in driving the PFIv2 in mid-latitudes. But north of the Arctic circle, its influence is damped by much cooler temperatures and reduced VPD. Changes in rainfall distribution and VPD/convection (figures 5(A) and (B)) are the main forcings that produce fire weather.

The interannual changes (STDs) in PFIv2 during July through October (JASO) are much larger in southern Europe and across Canada (figure 5(E)). The Pan-Arctic region has experienced substantial changes in mesoscale systems that modify daily Prec and temperature extremes [16]. Thus, fire vulnerability increases because it is much more related to Prec distribution in short intervals rather than the total accumulated rainfall throughout the season [3].

To evaluate PFIv2 characteristics in more detail, its components have also been computed based on ERA5. The hemispheric pattern of PFIv2 in ERA5 is like ASRv2 (figures 6(A) and S2). However, differences between the ASRv2 and ERA5 are greater north of 50° N, where ASRv2 shows more vulnerable conditions to fire occurrence. ASRv2 also highlights positive anomalies across southern Europe that indicate

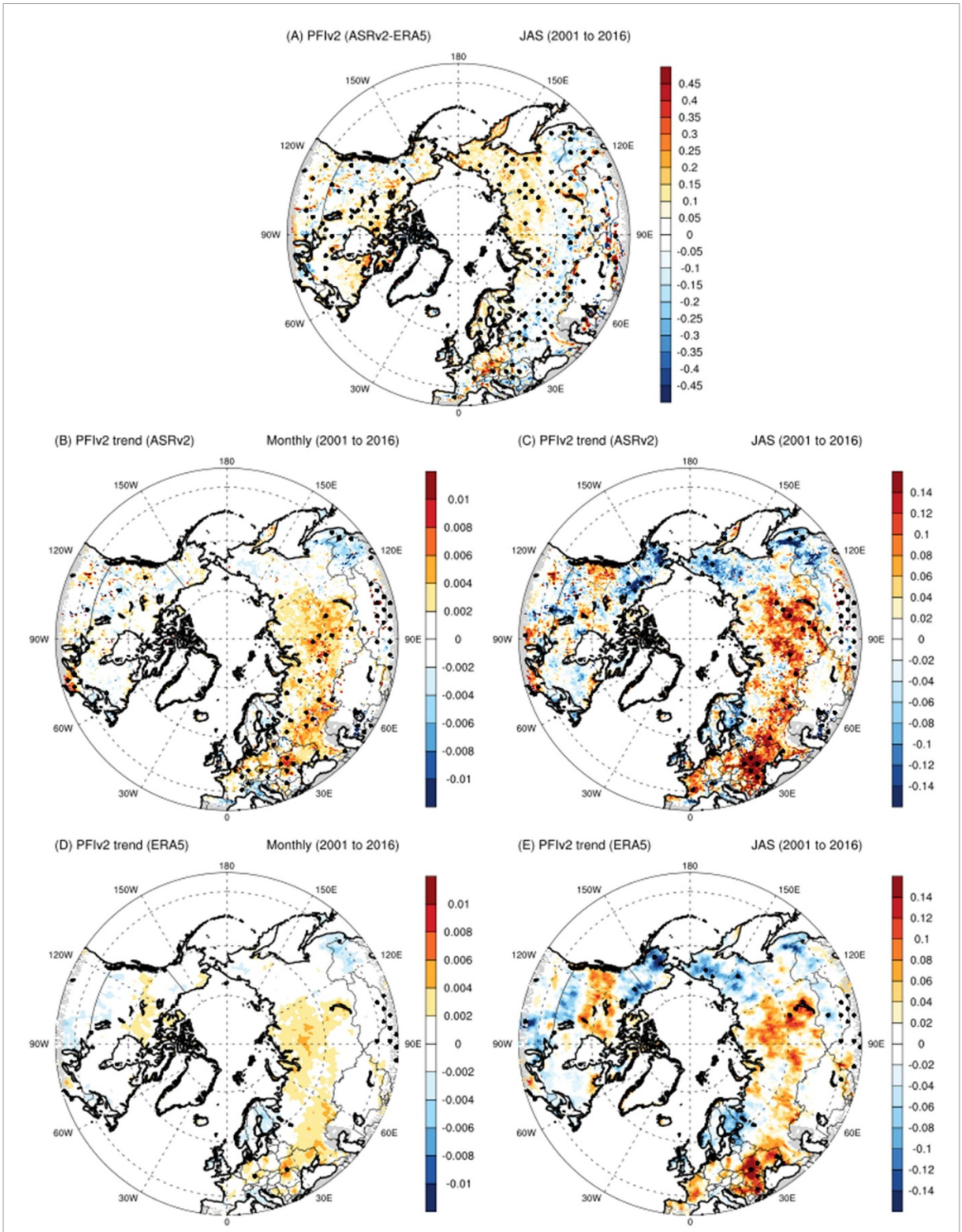

Figure 6. PFIv2 comparison using ASRv2 and ERA5. (A) Differences in PFIv2 based on ASRv2 and ERA5. (B) shows the PFIv2 trends for ASRv2 computed by including all months. (C) shows the PFIv2 trends only for the JAS (July–August–September) interval. (D) and (E) are the same as (B) and (C) but based on ERA5. Dotted regions are significant at 90% level.

the temporal distribution of Prec is more favorable to fire activity. Most of these differences between ASRv2 and ERA5 are statistically significant based on a Student's t-test, particularly over Russia and Scandinavia (figure 6(A)). Differences between ASRv2 and ERA5 over North America are smaller and generally not statistically significant. ASRv2 performs better concerning ERA5 when evaluated relative to observed fires in greater fire hazard areas. ASRv2 is warmer and drier than ERA5, as shown by the differences in the LogHai term and temperature factor of the PFIv2 (figure S2). This allows more vigorous upward air flow that increases the fire danger in ASRv2 (figure S2).

Turning to trends in PFIv2 (figures 6(B)–(E)), increased vulnerability to fire danger/danger is found across the Arctic and extratropics. This is primarily related to changes in daily Prec according to

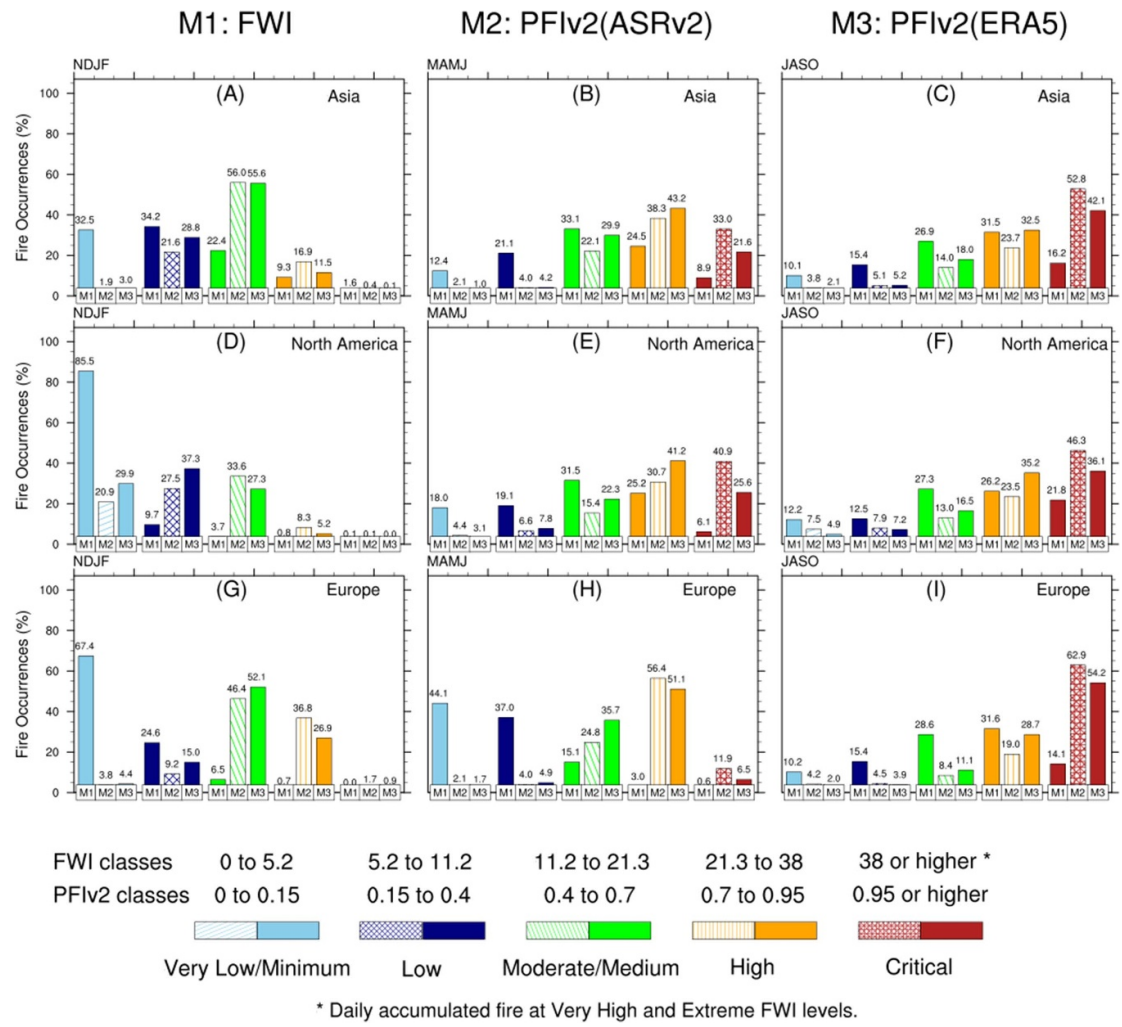

Figure 7. Percentage of daily accumulated fire at each PFIv2 class based on ASRv2, and ERA5 in MAMJ, JASO and NDJF months for 2001–2016. (A)–(C) Asia, (D) –(F) North America, and (G)–(I) Europe.

PFIv2 components. Positive trends are larger in the mid-latitudes of central Eurasia and Siberia, regions currently prone to fire activity. As shown by previous findings in North America, positive trends in temperature also increase fire susceptibility by reducing soil moisture and limiting vegetation's greening.

Northwestern North America and eastern Asia show negative PFIv2 trends that are minimally statistically significant (figures 6(B) and (D)). This feature is more prominent during the summer season as negative trends are not present in trends based on all months (figures 6(B) and (D)). This indicates an extension of the fire season [10] and an increase in fire danger in months other than JASO. Based on Normalized Difference Vegetation Index, previous investigations have shown that these areas of the Pan-Arctic have experienced positive growing season trends [37]. This greening at high latitudes does not favor increased fire danger due to available moisture in the canopy [18]. Pan-Arctic trends (1979–2019) computed for the Canadian Forest Fire Danger Rating System FWI derived from ERA5 [19] show very similar patterns as delivered by the PFIv2 based on ASRv2 and ERA5 datasets.

The skill of the PFIv2 to match MODIS detected-hot spots (fires) is analyzed based on ASRv2 and ERA5 input datasets (figure 7). The PFIv2 is also compared to the forest FWI system based on the ERA5 dataset used at ECMWF/Copernicus Climate Change Services. The FWI is extensively applied by National Weather Service worldwide to estimate fire danger.

Since the PFIv2 does not consider other factors (e.g. population density and lightning), results show that during NDJF, most fires are located within the medium or low danger classes of the PFIv2 (figures 7(A), (D) and (G)). In some instances, lightning discharge is intense enough to burn vegetation despite surface weather, climate, and vegetative conditions not typically prone to fire development according to the PFIv2. It is desirable that most fires should be found in areas of high and maximum weather fire danger (PFIv2), thus allowing local authorities and communities to develop more efficient measures to avoid human-induced fires. In

NDJF, it is clear that both datasets (ASRv2 and ERA5) show similar performance in locating fires, though ASRv2 locates more fires in the high and medium classes compared to ERA5 (figures 7(A), (D) and (G)).

Turning to the March–April–May–June (MAMJ, (figures 7(B), (E) and (H))) interval, greater correspondence between the fires and regions of critical/maximum fire danger in Asia, North America, and Europe is highlighted, with more than 75% of hot spots in areas of high PFIv2. In Europe, a low number of fires fall in the critical class of PFIv2, revealing the need for improvement in the method and/or in the daily Prec distribution as delivered by the reanalyses. On the other hand, in JASO, PFIv2 does a reasonable job placing most fires in critical danger regions (figures 7(C), (F) and (I)).

Comparison between PFIv2 and FWI (figure 7), both forced by the ERA5 dataset, reveals that the FWI cannot indicate regions with hot spots and high fire danger. It has been shown that FWI is suitable in fire assessment worldwide; however, this is not the case in the Pan-Arctic. This limited skill has also been found for the McArthur FDI, another fire danger estimate parameter. FDI and FWI have similar spatial patterns (not shown, [50]). It is evident that for FDI and FWI, most fires occur in regions of minimum and low fire danger/danger. By contrast, PFIv2 shows most fires occur in areas of high/critical danger conditions.

It is important to highlight that ASRv2 input data demonstrate greater skill in matching regions more prone to fire occurrence than ERA5. This is important because although hot-spots may happen in areas with low fire danger, their higher incidence is identified in drier and warmer conditions. Thus, advanced measures to reduce the fire hazards can be taken based on a prediction of fire danger, which at the continental scale should rely on reanalyses and other gridded datasets, or weather forecast models that in some locations are available only in low spatial resolution. Table S1 summarizes the values shown in figure 7.

Despite the increasing urgency to address average fire distribution and climate conditions, the reliability of the PFIv2, FDI, and FWI should also be verified for a series of extreme individual events. According to NOAA (www.noaa.gov/news/northern-hemisphere-just-had-its-hottest-summer-on-record), 2020 is the only NH summer warmer than 2019 on record. Subsequently, western North America and Europe show significantly more intense fire activity than the 2003–2019 average. Fires in the Eurasian Arctic were also unprecedented in 2019, according to the Copernicus Atmosphere Monitoring Service/European Centre for Medium-Range Weather Forecasts (https://atmosphere.copernicus.eu/another-active-year-arctic-wildfires).

A case study of March through October 2019 shows that areas with a high danger of fire are predominantly found in mid-latitudes and western North America in PFIv2 (figures 8(A), (B), (D) and (E)). However, these features are not as pronounced using FWI. Thus, FWI fails to match the regions with observed hot spots across a large portion of Asia (figures 8(C) and (F)). For instance, FWI values less than 20 across eastern Asia, Europe, and Siberia characterize areas of low fire danger.

To verify the capability of the PFIv2 to deal with fire weather characteristics, the locations of maximum fire danger are correlated to estimates of MODIS BAs [39]. This demonstrates that high correlations are found in mid-latitudes (not shown), in particular between 30 and 60° E. Northward of 50° N, there is an agreement between the PFIv2 and BA, but due to the weaker severity of fires, the spatial coverage correlation is confined to some regions of Canada and western North America. Weaker correlation values are found where fire does not primarily follow the annual cycle and is dominated by lightning or human action.

4. Discussion and concluding remarks

The Pan-Arctic region and its vicinity have experienced remarkable climate and weather fluctuations. Efforts have been made to understand these changes and project the potential impact of global warming on environmental conditions, biodiversity, and the livelihood of people. The present study, based on high resolution reanalyses (ASRv2 and ERA5) and MODIS products, shows that satellite-based fires depict very different spatial and temporal distributions of hot spots across North America, Europe, and Asia. The fire-weather conditions are characterized by positive trends northward of 40° N, especially across Eurasia. Wildfires are entirely dependent on weather, vegetation and human interference. The Arctic and extra-tropics show different characteristics across North America, Europe and Asia. It is demonstrated that regions with higher number of hotspots and higher wildfire danger are well correlated with the daily distribution of Prec and the background vegetation type.

This indicates the need to use high resolution datasets that can reproduce local responses to changes in land use and cover, such as their greening and browning. Despite the greening in the Arctic/extratropical vegetation, scars of browning have been found and attributed to the increased presence of fires. In the case of recurrent events, dominant vegetation patterns may change substantially toward more vulnerable conditions, further increasing the fire danger under extreme climate conditions as predicted to occur in a warming world.

Comparison between PFIv2 and FWI/FDI indices reveal that the latter do not reproduce areas with a high incidence of fire (FWI/FDI values are very low) across the Pan-Arctic region. This might be

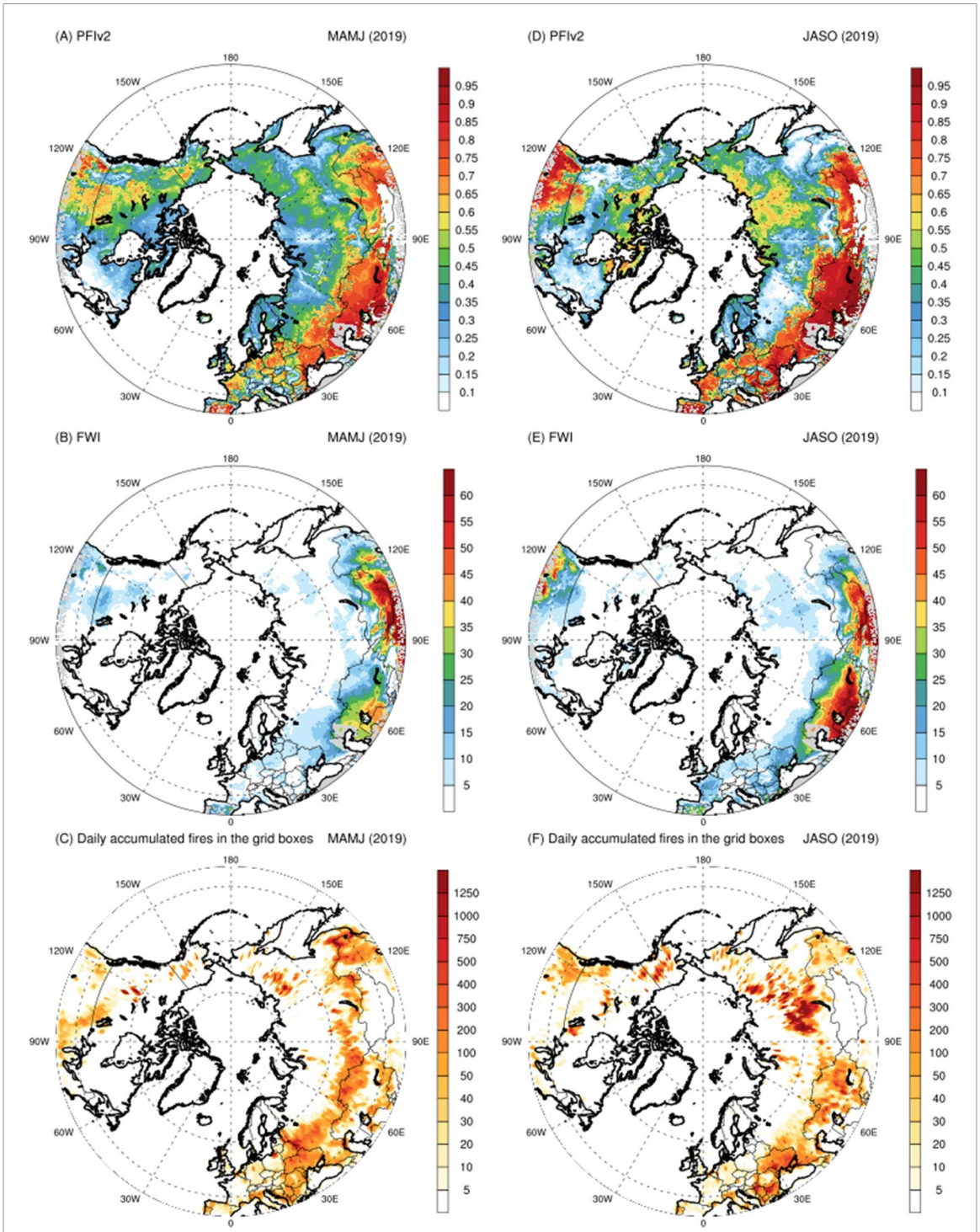

Figure 8. PFIv2 and FWI comparison of fire depiction in 2019. PFIv2 fire danger in (A) MAMJ and (D) JASO. (B) and (E) are the same as (A) and (D) except for FWI. (C) and (F) show daily satellite-observed accumulated hot spots in the grid boxes based on ERA5 in MAMJ and JASO, respectively.

related to the fact that the FWI/FDI assumes pine vegetation in all regions. However, climate conditions in the Pan-Arctic may not allow the development of combustible material related to this kind of vegetation. This limitation is surpassed using ASRv2, which updates the vegetation every 8 d throughout the 2001–2016 interval in the PFIv2. The PFIv2 methodology demonstrates a high capability to locate observed hot spots and can be applied to anticipate the potential of a particular region to develop erratic fires. Indeed, its application may be useful for authorities and society to minimize and hamper the adverse effect of the indiscriminate use of fire. However, the PFIv2 also shows limitations by excluding the influence of population density and lightning as a driver of fire incidence. These processes are complex, and little formulation exists to incorporate their impact because the population exhibits an individual manner to deal with fire, and lightning does not stimulate fires randomly [3]. For the time being, we must

cope with the remaining uncertainties it is necessary to intensify the understanding of those processes on global and local scales.

Data availability statement

Data beyond what is provided in the paper and/or the supplementary materials may be requested from the authors.

The data that support the findings of this study are available upon reasonable request from the authors.

Acknowledgments

This study was supported by The National Council for Scientific and Technological Development (CNPq), Fundacão de Amparo a Pesquisa do Estado de Minas Gerais (FAPEMIG), and the Byrd Polar and Climate Research Center of which this is contribution number 1604. AF is funded by ANID-FONDECYT grant number 1201429. We highlight useful discussion with the Polar Meteorology Group on the Arctic climate as well as we thank Dr. Alberto Setzer for idealization of the first version of the PFI.

Conflict of interest

The authors declare that they have no competing interests.

ORCID iDs

Flavio Justino https://orcid.org/0000-0003-0929-1388
Alex Silva https://orcid.org/0000-0002-6365-5659
Alvaro Avila-Diaz https://orcid.org/0000-0002-0404-4559

References

[1] Meyn A, White P S, Buhk C and Jentsch A 2007 Environmental drivers of large, infrequent wildfires: the emerging conceptual model *Prog. Phys. Geogr. Earth Environ.* **31** 287–312
[2] Bowman D M J S *et al* 2009 Fire in the earth system *Science* **324** 481–4
[3] Silva A S, Justino F, Setzer A W and Avila-Diaz A 2021 Vegetation fire activity and the Potential Fire Index (PFIv2) performance in the last two decades (2001–2016) *Int. J. Climatol.* **41** 78–92
[4] Hantson S *et al* 2020 Quantitative assessment of fire and vegetation properties in simulations with fire-enabled vegetation models from the fire model intercomparison project *Geosci. Model. Dev.* **13** 3299–318
[5] Andela N *et al* 2017 A human-driven decline in global burned area *Science* **356** 1356–62
[6] Veraverbeke S, Rogers B M, Goulden M L, Jandt R R, Miller C E, Wiggins E B and Randerson J T 2017 Lightning as a major driver of recent large fire years in North American boreal forests *Nat. Clim. Change* **7** 529–34
[7] Bowman D M J S, Kolden C A, Abatzoglou J T, Johnston F H, Van Der Werf G R and Flannigan M 2020 Vegetation fires in the anthropocene *Nat. Rev. Earth Environ.* **1** 500–15
[8] Rocha A V, Loranty M M, Higuera P E, Mack M C, Hu F S, Jones B M, Breen A L, Rastetter E B, Goetz S J and Shaver G R 2012 The footprint of Alaskan tundra fires during the past half-century: implications for surface properties and radiative forcing *Environ. Res. Lett.* **7** 44039–47
[9] Kim J S, Kug J S, Jeong S J, Park H and Schaepman-Strub G 2020 Extensive fires in southeastern Siberian permafrost linked to preceding Arctic oscillation *Sci. Adv.* **6** eaax3308
[10] Masrur A, Petrov A N and DeGroote J 2018 Circumpolar spatio-temporal patterns and contributing climatic factors of wildfire activity in the Arctic tundra from 2001–2015 *Environ. Res. Lett.* **13** 14019–30
[11] Krawchuk M A, Moritz M A, Parisien M A, Van Dorn J and Hayhoe K 2009 Global pyrogeography: the current and future distribution of Wildfire ed J Chave *PLoS One* **4** e5102–14
[12] Wittich K P 2005 A single-layer litter-moisture model for estimating forest-fire danger *Meteorol. Z.* **14** 157–64
[13] Huang X and Rein G 2015 Computational study of critical moisture and depth of burn in peat fires *Int. J. Wildland Fire* **24** 798–808
[14] Scheiter S and Higgins S I 2009 Impacts of climate change on the vegetation of Africa: an adaptive dynamic vegetation modelling approach *Glob. Change Biol.* **15** 2224–46
[15] Post E *et al* 2019 The polar regions in a 2°C warmer world *Sci. Adv.* **5** 1–12
[16] Avila-Diaz A, Bromwich D H, Wilson A B, Justino F and Wang S H 2021 Climate extremes across the North American Arctic in modern reanalyses *J. Clim.* **34** 2385–410
[17] Zhang J and Wang F 2019 Changes in the risk of extreme climate events over East Asia at different global warming levels *Water* **11** 2535–47
[18] Myers-Smith I H *et al* 2020 Complexity revealed in the greening of the Arctic *Nat. Clim. Change* **10** 106–17
[19] Albergel C, Dutra E, Munier S, Calvet J C, Munoz-Sabater J, De Rosnay P and Balsamo G 2018 ERA-5 and ERA-interim driven ISBA land surface model simulations: which one performs better? *Hydrol. Earth Syst. Sci.* **22** 3515–32
[20] Bromwich D *et al* 2018 The arctic system reanalysis, version 2 *Bull. Am. Meteorol. Soc.* **99** 805–28
[21] Friedlingstein P *et al* 2019 Global carbon budget 2019 *Earth Syst. Sci. Data* **11** 1783–838
[22] Van Wagner C E 1987 Development and structure of the Canadian forest fire weather index system *Can. For. Ser. For. Tech. Rep.* **35** 37 (https://cfs.nrcan.gc.ca/pubwarehouse/pdfs/19927.pdf)
[23] Giglio L, Schroeder W and Justice C O 2016 The collection 6 MODIS active fire detection algorithm and fire products *Remote Sens. Environ.* **178** 31–41
[24] Roteta E, Bastarrika A, Padilla M, Storm T and Chuvieco E 2019 Development of a Sentinel-2 burned area algorithm: generation of a small fire database for sub-Saharan Africa *Remote Sens. Environ.* **222** 1–17
[25] Cusworth D H, Mickley L J, Sulprizio M P, Liu T, Marlier M E, DeFries R S, Guttikunda S K and Gupta P 2018 Quantifying the influence of agricultural fires in northwest India on urban air pollution in Delhi, India *Environ. Res. Lett.* **13** 044018
[26] Pettitt A N 1979 A non-parametric approach to the change-point problem *Appl. Stat.* **28** 126–35
[27] Sen P K 1968 Estimates of the regression coefficient based on Kendall's tau *J. Am. Stat. Assoc.* **63** 1379–89
[28] Hamed K H and Rao A 1998 A modified Mann-Kendall trend test for autocorrelated data *J. Hydrol.* **204** 182–96
[29] Zhao K *et al* 2019 Detecting change-point, trend, and seasonality in satellite time series data to track abrupt changes and nonlinear dynamics: a Bayesian ensemble algorithm *Remote Sens. Environ.* **232** 111181–201
[30] Barlow M *et al* 2019 North American extreme precipitation events and related large-scale meteorological patterns: a review of statistical methods, dynamics, modeling, and trends *Clim. Dyn.* **53** 6835–75

[31] Zuluaga C F, Avila-Diaz A, Justino F B and Wilson A B 2021 Climatology and trends of downward shortwave radiation over Brazil *Atmos. Res.* **250** 105347
[32] Pan N, Feng X, Fu B, Wang S, Ji F and Pan S 2018 Increasing global vegetation browning hidden in overall vegetation greening: insights from time-varying trends *Remote Sens. Environ.* **214** 59–72
[33] NOAA 2020 Global climate Report—annual 2010 (available at: www.ncdc.noaa.gov/sotc/global/201013)
[34] NOAA 2020 Drought—annual 2002 (available at: www.ncdc.noaa.gov/sotc/drought/200213).
[35] Yuan W *et al* 2019 Increased atmospheric vapor pressure deficit reduces global vegetation growth *Sci. Adv.* **5** 1396–408
[36] Zhang Y *et al* 2016 Multi-decadal trends in global terrestrial evapotranspiration and its components *Sci. Rep.* **6** 19124–35
[37] Guay K C, Goetz S J and Beck P S A 2015 Long-term arctic growing season NDVI trends from GIMMS 3g, 1982–2012 *ORNL DAAC* (https://doi.org/10.3334/ORNLDAAC/1275)
[38] Pan N, Feng X, Fu B-J, Wang S, Ji F and Pan S 2018 Increasing global vegetation browning hidden in overall vegetation greening: insights from time-varying trends *Remote Sens. Environ.* **214** 59–72
[39] ORNL DAAC, MODIS and VIIRS L 2018 VIIRS land products global subsetting and visualization tool *ORNL Distrib. Act. Arch. Cent.* (https://doi.org/10.3334/ORNLDAAC/1379)